Molecular Vision 2013; 19:2561-2570 <http://www.molvis.org/molvis/v19/2561>
Received 16 August 2013 | Accepted 12 December 2013 | Published 16 December 2013

Contractile markers distinguish structures of the mouse aqueous drainage tract

MinHee K. Ko, James C.H. Tan

Doheny Eye Institute and Department of Ophthalmology, Keck School of Medicine University of Southern California, Los Angeles CA

Purpose: Structures of the aqueous humor drainage tract are contractile, although the tract is not entirely composed of muscle. We characterized the mouse aqueous drainage tract by immunolabeling contractile markers and determined whether profiling these markers within the tract distinguished its key structures of the trabecular meshwork (TM) and ciliary muscle (CM).

Methods: Enucleated eyes from pigmented C57BL/6 (n=8 mice) and albino BALB/c (n=6 mice) mice were processed for cryo- and formalin-fixed paraffin-embedded sectioning. Immunofluorescence labeling was performed for the following: (a) filamentous actin (using fluorescence-conjugated phalloidin), representing a global contractile marker; (b) α-smooth muscle actin (α-SMA), caldesmon, and calponin, representing classic smooth muscle epitopes; and (c) nonmuscle myosin heavy chain, representing a nonmuscle contractile protein. Tissue labeling was identified by confocal microscopy and analyzed quantitatively. Hematoxylin and eosin staining provided structural orientation.

Results: A small portion of the TM faced the anterior chamber; the rest extended posteriorly alongside Schlemm's canal (SC) within the inner sclera. Within the drainage tract, filamentous actin labeling was positive in TM and CM. α-SMA and caldesmon labeling was seen primarily along the CM, which extended from the anterior chamber angle to its posterior termination beyond the SC near the retina. Low intensity, patchy α-SMA and caldesmon labeling was seen in the TM. Myosin heavy chain immunoreactivity was primarily found in the TM and calponin was primarily observed in the CM. C57BL/6 and BALB/c comparison showed that pigment obscured fluorescence in the ciliary body.

Conclusions: Our strategy of profiling contractile markers distinguished mouse aqueous drainage tract structures that were otherwise indistinguishable by hematoxylin and eosin staining. The mouse TM was seen as an intervening structure between SC, a part of the conventional drainage tract, and CM, a part of the unconventional drainage tract. Our findings provide important insights into the structural and functional organization of the mouse aqueous drainage tract and a basis for exploring the role of contractility in modulating aqueous outflow.

Contractility by structures of the primate aqueous humor drainage tract modulates aqueous outflow and intraocular pressure (IOP) [1,2]. Organization of the mouse aqueous drainage tract has not been fully characterized, but it is thought to mimic that of primates [3]. This organization is worth studying, as it potentially provides a basis for understanding contractile function in the mouse aqueous drainage tract. It could also provide important insights into IOP regulation, glaucoma pathogenesis, and the development of novel glaucoma therapy.

Key contractile structures of the aqueous drainage tract are the trabecular meshwork (TM), a nonmuscle tissue, and ciliary muscle (CM), which is smooth muscle. As with primates, mice have a lamellated TM with layers of cells [1,4]. The TM allows aqueous drainage into Schlemm's canal (SC), forming the equivalent of a conventional outflow pathway. The TM in primates is contractile, with contractility mediated by a highly organized nonmuscle actomyosin system comprising actin microfilaments, actin-associated proteins, and myosin molecular motors [1,2,5]. The actomyosin system plays essential roles in regulating cell–extracellular matrix interactions that modulate aqueous humor drainage and IOP. It is not clear whether similar contractile elements are present in the TM of mice in vivo [4,6].

The CM is smooth muscle under autonomic influence. Classic smooth muscle markers such as α-smooth muscle actin (α-SMA), caldesmon, and calponin are expressed in the CM of primates [7-10]; whether this is also true in mice has not been established in situ. Although the TM is not considered smooth muscle, expression of smooth muscle markers such as α-SMA may be seen in the TM [8-10].

There is evidence of an alternative, unconventional pathway in mice and aqueous drainage through this pathway is suggested to play a bigger role in outflow in mice than primates [11,12]. In primates, the CM forms the anterior part

Correspondence to: James C.H. Tan, Doheny Eye Institute and Department of Ophthalmology, Keck School of Medicine, University of Southern California, Los Angeles CA 90033; Phone: (323) 442-6415; FAX: (323) 442-6412; email: minheeki@usc.edu and oranghutan@aol.com

of the unconventional outflow pathway that continues posteriorly in the suprachoroidal space. Primate CM contractility allows for outflow modulation through the conventional and unconventional routes [13-16], but it is unknown whether this interaction occurs in mice. In mice, the precise relationships between the TM, CM, and SC within the aqueous drainage tract are unclear. These relationships are worth knowing, as they will provide a structural basis for understanding the role of contractility in aqueous outflow dynamics, which in turn has important implications for understanding IOP regulation.

In the present study, we sought to characterize the contractile apparatus of the mouse aqueous drainage tracts by immunolabeling contractile markers of the drainage tissues. We examined immunolocalization of markers of global contractility (polymerized actin), classic smooth muscle epitopes (α-SMA, caldesmon, and calponin) and nonmuscle contractile proteins (nonmuscle myosin heavy chain [MHC]) in the aqueous drainage tract. We hypothesized that profiling these markers in the tissue would allow the TM and CM to be distinguished in C57BL/6 mice, a widely used background strain for engineered mice. We also examined a second mouse strain, albino BALB/c mice, to guide interpretation of fluorescent labeling within the pigmented anterior uvea.

METHODS

Animals: Animal care and use was in compliance with institutional guidelines and with the Association for Research in Vision and Ophthalmology Statement for the Use of Animals in Ophthalmic and Vision Research. C57BL/6 and BALB/c mice (n=6–8 mice of each strain, 6–8 weeks old) were purchased from Charles River Laboratories International, Inc. (Wilmington, MA). Animals were stored in a temperature-controlled room with a 12h:12h light-dark cycle and fed ad libitum.

Reagents: Alexa Fluor 568–conjugated phalloidin and ProLong Gold Anti-fade with 4',6-diamidino-2-phenylindole were purchased from Life Technologies (Grand Island, NY). Tissue-Tek optimum cutting temperature compound was purchased from Sakura Finetek (Torrance, CA). Paraformaldehyde, Triton X-100, and bovine serum albumin were purchased from Sigma (St. Louis, MO).

Antibodies: Alexa Fluor 488-, 568-, or 633–conjugated secondary antibodies were purchased from Life Technologies. Rabbit or goat anti-α-SMA (Cat # ab5694 or ab21027, 1:100 dilution), mouse anti-MHC nonmuscle (Clone 3H2, Cat # ab684, 1:200 dilution), rabbit anti-caldesmon (E89, Cat # ab32330, 1:200 dilution), and rabbit anti-calponin (Clone EP798Y, Cat# ab5694, 1:100 dilution) were purchased from Abcam (Cambridge, MA). Normal goat, rabbit, and mouse immunoglobulin G isotypes were purchased from Santa Cruz Biotechnology, Inc. (Santa Cruz, CA).

Immunofluorescence staining: Enucleated eyes were quickly embedded in Tissue-Tek optimum cutting temperature compound. Cryosections (7 µm thickness) were fixed with 4% paraformaldehyde and further permeabilized/blocked in the blocking solution (5% bovine serum albumin and 0.3% Triton X-100) for 1 h at room temperature. Sections were incubated overnight at 4 °C with combinations of primary antibodies (single, dual, or triple) in the blocking solution. The sections were further incubated for 1 h at room temperature with a combination of secondary antibodies, Alexa Fluor–conjugated anti-rabbit, mouse, and/or goat antibodies, and then mounted using ProLong Gold Anti-fade reagent with 4',6-diamidino-2-phenylindole. To visualize polymerized actin, sections were subsequently incubated with Alexa 568–phalloidin along with the appropriate combination of secondary antibodies. Negative, nonspecific labeling was established with normal immunoglobulin G isotypes. Antibody specificity was confirmed by immunoreactivity in blood vessels and extraocular muscle in the same sections used for primary labeling, which provided internal positive controls. Sections were analyzed with a Leica SP5 high-speed spectral confocal laser-scanning microscope (Leica Microsystems, Wetzlar, Germany) or a Zeiss LSM 710 confocal microscope (Carl Zeiss, Oberkochen, Germany). Immunofluorescence staining for single or double contractile markers was performed using randomly selected slides (4–5 slides per each eye) containing four sections per slide and examined under the confocal microscope. Additional cryosections and formalin-fixed paraffin-embedded tissue sections (FFPE) were stained with hematoxylin and eosin (H&E) and examined by light microscopy for morphology.

Quantification and stereological counting procedure: Specific fluorescence from tissue labeling in histological sections was captured by confocal microscopy with exposure time kept constant across all images. Image sections were imported as 16 bit images and analyzed by NIH Image J software. Fluorescence intensity of pixel gray values in eight separate regions of interest (ROIs) per region of TM and CM was calculated and averaged across each tissue region. This was performed separately for each label (filamentous actin [F-actin], α-SMA, MHC, caldesmon, and calponin) in TM and CM and averaged across data from three mice. Fluorescence intensity for F-actin, α-SMA, MHC, caldesmon, and calponin in the TM and CM were then compared using analysis of variance (ANOVA) and Tukey's and Sidak's comparison tests.

Figure 1. Histological features of mouse aqueous drainage tissue based on hematoxylin and eosin (H&E) staining. Enucleated eyes of C57BL/6 mice were embedded in formalin-fixed paraffin embedded sections then H&E stained. Opened arrows indicate ciliary muscle; closed arrows indicate trabecular meshwork; asterisk (*) indicates Schlemm's cannal. Scale bars, 20 µm.

RESULTS

Aqueous drainage tract histology in C57BL/6 mice: The TM begins anteriorly at the termination of the corneal endothelium, where the corneal endothelial monolayer transitions to a multilayered cellular structure in the iridocorneal angle, as shown in Figure 1. This part of the TM becomes pigmented near the apex of the iridocorneal angle and iris root. SC starts just posterior to the iridocorneal angle and adjacent to the pigmented TM in the angle. The TM continues as a multilayered cellular structure right next to SC deeper in the inner sclera until SC terminates posteriorly just beyond the ciliary processes.

The CM is identifiable posteriorly near the anterior termination of the retina. It borders ciliary body (CB) pigment. The expected anterior extension of the CM in between the tissue planes of the pigmented CB and TM is hard to identify in H&E sections.

Filamentous actin labeling in C57BL/6 mice: In C57BL/6 mice, phalloidin labeling of F-actin in the aqueous drainage tract was strongly positive in a band, consistent with CM adjacent to the pigmented CB, as shown in Figure 2A. CM F-actin labeling was broadest and most intense posteriorly near the anterior termination of retina. More anterior CM labeling extended alongside the pigmented CB (open arrows). TM F-actin labeling was seen in the TM region adjacent to the corneal endothelium and in inner scleral aspects of the TM adjacent to SC (closed arrows).

Overall, F-actin labeling was seen in both CM and TM, albeit less intensely in TM. It was hard to distinguish between the structures of TM and CM by F-actin labeling alone.

α-Smooth muscle actin and caldesmon immunolocalization in the ciliary muscle and trabecular meshwork: Positive α-SMA labeling was seen in the CM, as shown in Figure 3A. α-SMA labeling formed a bright band in the posterior regions of the CM (open arrows) and a thin and wavy structure adjacent to the pigmented CB and anteriorly near the iridocorneal angle (arrowhead; Figure 3A). α-SMA labeling was positive but spotty in the cellular layers of the TM next to SC. F-actin and α-SMA labeling clearly colocalized in the CM. F-actin and α-SMA co-localization was patchy and less apparent in TM cellular layers adjacent to SC (dotted outline in Figure 3F; high power).

Positive caldesmon labeling was seen in the TM (closed arrows; Figure 4A) and CM (open arrows; Figure 4A). In the CM, caldesmon labeling was present in its posterior portion and more anteriorly next to the pigmented CB, seen as a thin streak extending to the iridocorneal angle. Weaker, speckled caldesmon labeling was present in TM cellular layers next to SC, and also more anterior portions of TM starting at the terminus of corneal endothelium. F-actin and caldesmon colocalization was seen primarily in the CM (yellow; Figure

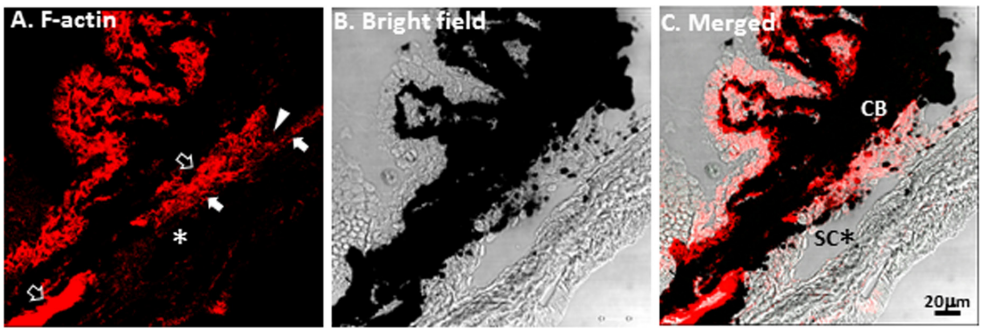

Figure 2. Phalloidin labeling of filamentous actin (F-actin) in C57BL/6 mouse aqueous drainage tract. **A**: positive F-actin labeling (red) was seen in the ciliary muscle (opened arrows) adjacent to the pigmented ciliary body (CB) and trabecular meshwork (TM; closed arrows). F-actin labeling was positive in the TM extending from the iridocorneal angle (arrowhead) and alongside SC (asterisk *). **B** and **C**: Merged bright field-fluorescence images provide detailed structural orientation. Scale bars, 20 µm.

4C,F), with colocalization spotty in TM cellular layers adjacent to SC (dotted outline in Figure 4F; high power).

Non-muscle myosin heavy chain immunolocalization in the trabecular meshwork: Positive non-muscle MHC labeling was primarily observed in the TM (closed arrows; Figure 5A), as seen in cellular layers adjacent to SC and the corneal endothelium terminus at the iridocorneal angle (arrowhead; Figure 5A). MHC labeling intensity was relatively low in the CM, especially posteriorly, relative to positive F-actin labeling in the CM (opened arrows; Figure 5C,F). Patchy co-localization of MHC and F-actin was seen in TM cellular layers adjacent to SC (dotted outline; Figure 5C,F).

Calponin immunolocalization in ciliary muscle: Positive calponin labeling was seen in the CM (open arrows) posteriorly and in more anterior CM regions adjacent to the pigmented CB, as shown in Figure 6. Calponin colocalized with F-actin in the CM. Very limited or no calponin labeling was present in TM (closed arrows) cellular layers next to SC, where only occasional spotty calponin colocalization with F-actin was seen (next to the dotted outline of SC; Figure 6E,F)

Primary immunolocalization of α-smooth muscle actin, caldesmon, nonmuscle myosin heavy chain, and calponin distinguish ciliary muscle and trabecular meshwork: Primary immunolocalization of α-SMA (Figure 7A,E), caldesmon

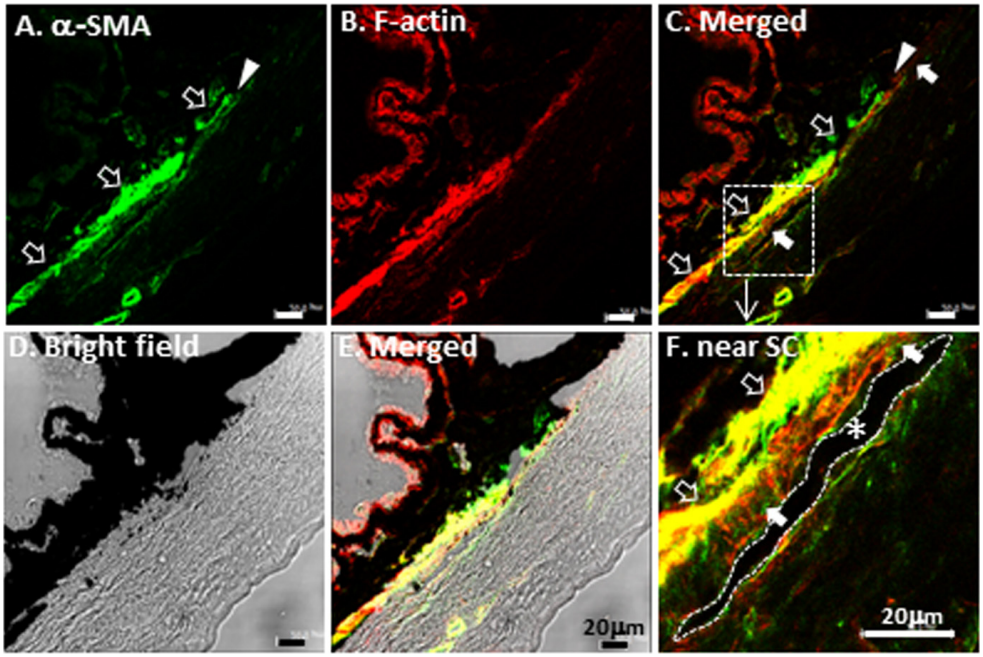

Figure 3. α-Smooth muscle actin (SMA) and F-actin immunolocalization in the trabecular meshwork (TM) and ciliary muscle (CM). **A**: Positive α-SMA labeling was seen in posterior regions of the CM (opened arrows) and anteriorly near the iridocorneal angle (arrowhead). **B**: Positive F-actin labeling (red) was seen in ciliary processes, CM and TM. **C**: Co-localization of F-actin and α-SMA labeling. α-SMA labeling was positive but of low intensity and patchy in cellular layers of the TM (closed arrows). **D**: Bright field for tissue orientation. **E**: Merged bright field and fluorescence images provide detailed structural orientation. **F**: Magnified image of dotted square of **C**: F-actin and α-SMA co-localization was intense in the CM, but patchy and less apparent in TM cellular layers adjacent to SC (dotted outline, asterisk*). Scale bars, 20 µm.

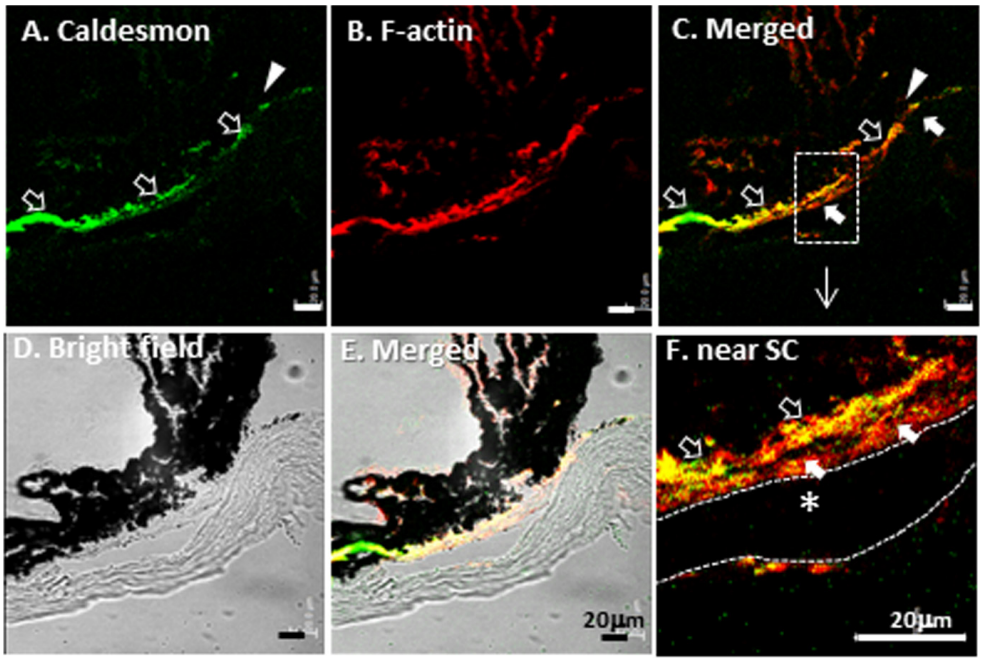

Figure 4. Caldesmon and F-actin immunolocalization in the trabecular meshwork (TM) and ciliary muscle (CM). **A**: Positive caldesmon labeling was present in its posterior portion of the CM (opened arrows) with extension to the iridocorneal angle (arrowhead). **B**: Positive F-actin labeling (red) was seen in in ciliary processes, CM and TM. **C**: F-actin and caldesmon co-localization was seen primarily in the CM (opened arrows, yellow), with co-localization more spotty in the TM (closed arrows, red). **D**: Bright field for tissue orientation. **E**: Merged bright field and fluorescence images provide detailed structural orientation. **F**: Magnified image of dotted square of **C** showed that F-actin and caldesmon co-localization was seen primarily in the CM (yellow; opened arrows). In the TM next to SC (dotted outline, asterisk *), caldesmon and F-actin co-localization was spotty (closed arrows). Scale bars, 20 µm.

(Figure 7B), calponin (Figure 7I), and nonmuscle MHC (Figure 7F,J) were exhibited in different regions of the aqueous drainage tract. α-SMA labeled the CM primarily, extending from a broad band of CM labeling posteriorly to a thinner, wavy band of labeling anteriorly and adjacent to the pigmented CB, as shown in Figure 7A,E. α-SMA and

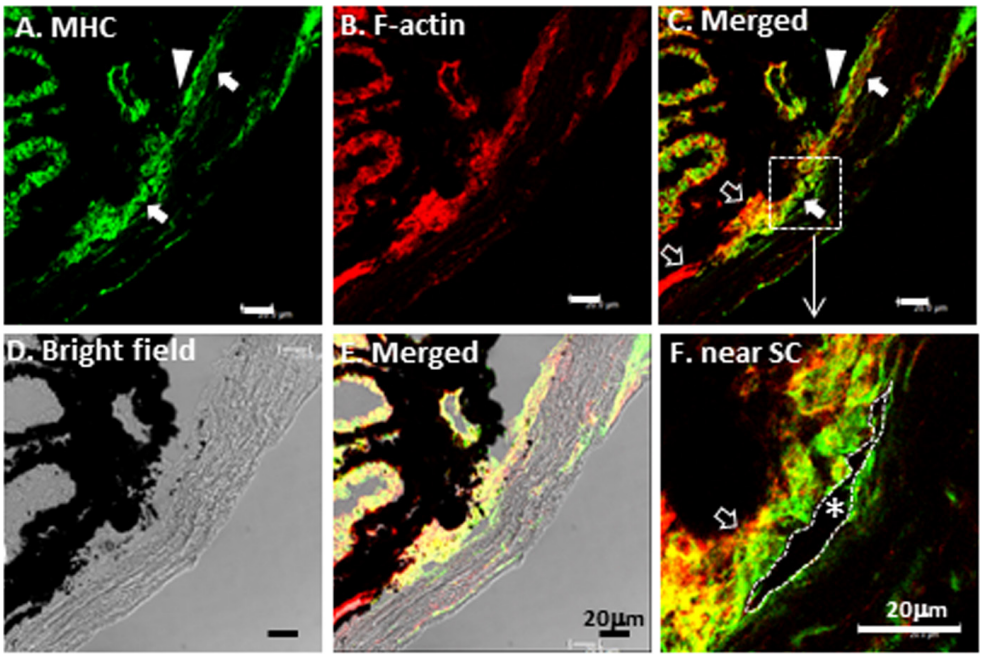

Figure 5. Non-muscle myosin heavy chain (MHC) and F-actin immunolocalization in trabecular meshwork (TM) and ciliary muscle (CM). **A**: Positive MHC labeling was primarily in the TM (closed arrows). MHC labeling was of relatively low intensity or absent in the CM (opened arrows), especially posteriorly. **B**: Positive F-actin labeling (red) was seen in ciliary processes, CM and TM. **C**: Patchy co-localization of MHC and F-actin was seen in TM cellular layers. **D**: Bright field for tissue orientation. **E**: Merged bright field and fluorescence images provide detailed structural orientation. **F**: Magnified image of dotted square of **C** showed co-localization of MHC and F-actin in CM. In the TM, adjacent to SC (dotted outline with asterisk*), MHC and F-actin co-localization was spotty. Scale bars, 20 µm.

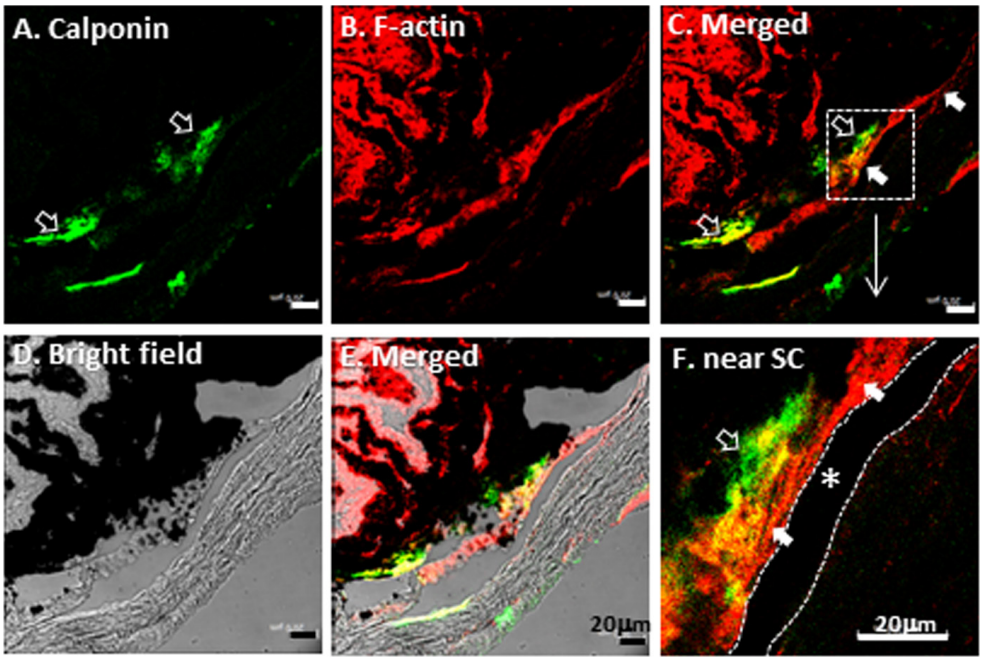

Figure 6. Calponin and F-actin immunolocalization in the trabecular meshwork (TM) and ciliary muscle (CM). **A**: Positive calponin labeling was seen in the CM posteriorly (opened arrows). **B**: Positive F-actin labeling (red) was seen in ciliary processes, CM and TM. **C**: Calponin co-localized with F-actin in the CM. **D**: Bright field for tissue orientation. **E**: merged bright field and fluorescence images provide detailed structural orientation. **F**: Magnified image of dotted square of **C** showed only spotty calponin co-localization with F-actin in TM cellular layers next to SC (dotted outline, asterisk*). Scale bars, 20 µm.

caldesmon colocalization was seen primarily in the CM, with spotty colocalization in the TM (Figure 7C). α-SMA and calponin labeling in TM cellular layers adjacent to SC were of low intensity and speckled, and colocalization with MHC here was minimal and spotty (Figure 7G,K). Hence, primary immunolocalization of α-SMA and calponin (primarily the CM), and of MHC (primarily the TM) was mostly separate, allowing structures of the CM and TM to be distinguished in the aqueous drainage tract. Immunolocalization of these markers in the CM (opened arrows) was distinct from that of nonmuscle MHC, which primarily labeled TM (closed arrows), as shown in Figure 7K.

Contractile markers in trabecular meshwork and ciliary muscle of albino BALB/c mice: Contractile marker labeling that was performed in the C57BL/6 aqueous drainage tract was repeated in albino BALB/c mice lacking pigment in order to determine whether pigment obscured interpretation of the CM. In BALB/c mice (n=6), a reticular pattern of F-actin and MHC was seen in the CB, which was otherwise

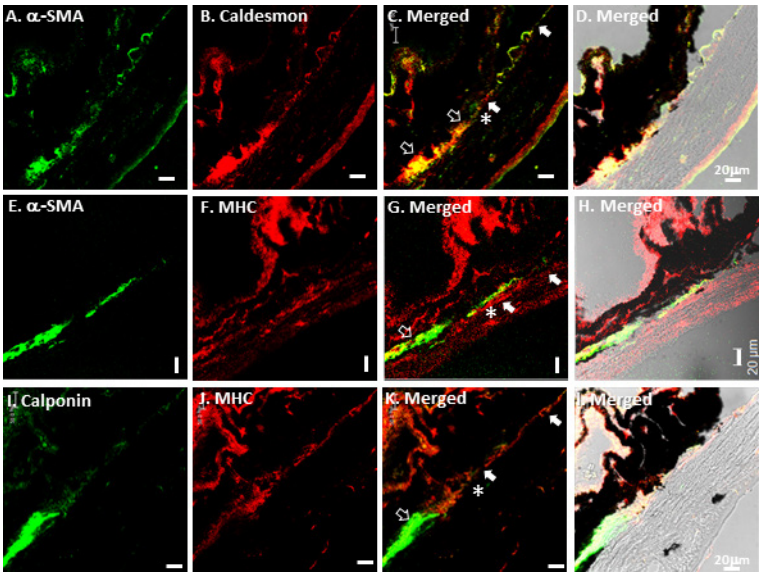

Figure 7. Primary immunolocalization of α-SMA, caldesmon, calponin, and MHC in the trabecular meshwork (TM) and ciliary muscle (CM). **A-D**: colocalization of α-SMA and caldesmon was primarily in CM (open arrow, yellow). **E-H**: α-SMA was mainly localized in CM (opened arrow, green), while MHC was mainly localized in the TM (closed arrows) adjacent to SC (asterisk *). **I-L**: calponin was mainly localized in CM (opened arrow, green), while MHC was mainly localized in the TM (closed arrows) adjacent to Schlemm's canal (SC; asterisk *). Scale bars, 20 µm.

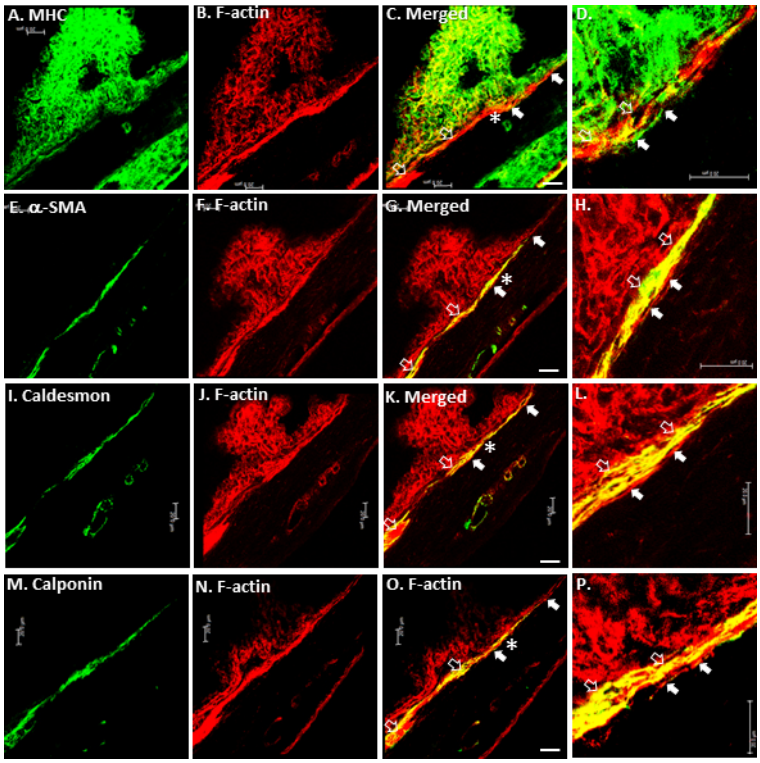

Figure 8. Contractile features of BALB/c mouse aqueous drainage tract. **A**-**C**: Reticular pattern of MHC and F-actin labeling was seen in the ciliary body (CB) of BALB/c mice (n=6), which was otherwise obscured by pigment in C57BL/6 mice. **D**: MHC was mainly localized in trabecular meshwork (TM; closed arrows) adjacent to Schlemm's canal (SC; asterisk*). **E**, **I**, **M**: the pattern of α-SMA, caldesmon, and calponin labeling in BALB/c mice was similar to that of C57BL/6 mice, confirming that pigment did not obscure interpretation of the CM in C57BL/6 mice. **H**, **L**, **P**: TM F-actin labeling in the TM adjacent to SC (asterisk*) did not co-localize with a-SMA, caldesmon or calponin (mainly closed CM). Scale bars, 20 µm.

obscured by pigment in C57BL/6 mice (Figure 8A,B,F,J,N). The pattern of α-SMA, caldesmon, and calponin labeling in the CM of BALB/c mice was similar to that in C57BL/6 mice, confirming that pigment did not obscure interpretation of the CM in C57BL/6 mice (Figure 8E,I,M). Colocalization of F-actin with α-SMA, caldesmon, and calponin was mainly seen in the CM (open arrows), while MHC showed partial colocalization with F-actin in the CM and TM (Figure 8C,D,G,H,K,L,O,P), confirming that the colocalization pattern of contractile markers was similar in both C57BL/6 and BALB/c mice.

Negative controls for each antibody were isotype controls and controls in which the primary antibody was omitted; these showed no specific reactivity (data not shown). Antibody specificity was confirmed in internal positive controls in the same sections. This comprised positive labeling of the intramural smooth muscle of extraocular blood vessels, wherein specific immunoreactivity was confirmed (data not shown).

Features of contractile markers in the trabecular meshwork and ciliary muscle: Figure 9 shows the extent of positive labeling for contractile markers, as quantified by fluorescence intensity measurements for each label in the aqueous drainage tissues of C57BL/6 mice. In the CM, mean fluorescence intensity was greatest for F-actin and least for MHC. CM MHC fluorescence intensity was significantly less than that of F-actin ($p=0.2$; one-way ANOVA and Tukey's comparison test). In the TM, mean fluorescence intensity was greatest for MHC and least for calponin. The TM fluorescence intensities of α-SMA, caldesmon, and calponin were less than those of F-actin and MHC ($p=0.0006$; one-way ANOVA and Tukey's comparison test). Fluorescence intensities of F-actin and classic smooth muscle markers, caldesmon, α-SMA and calponin, were significantly higher in the CM compared with the TM ($p<0.0001$; two-way ANOVA and Sidaki's comparison test). MHC fluorescence intensity in the TM and CM was similar ($p>0.05$).

DISCUSSION

Structures of the aqueous drainage tract such as the TM and CM are derived from the neural crest [17,18]. They may form a structural continuum, but lack easily identifiable histological boundaries, making it hard to distinguish one structure from another. The TM, part of the conventional outflow pathway, and CM, part of the unconventional pathway, are contractile structures of different types. The CM is smooth muscle, whereas the TM is nonmuscle tissue. We sought to distinguish the CM and TM by profiling different contractile markers in the aqueous drainage tissues of C57BL/6 mice, which are a potentially useful model for studying the aqueous

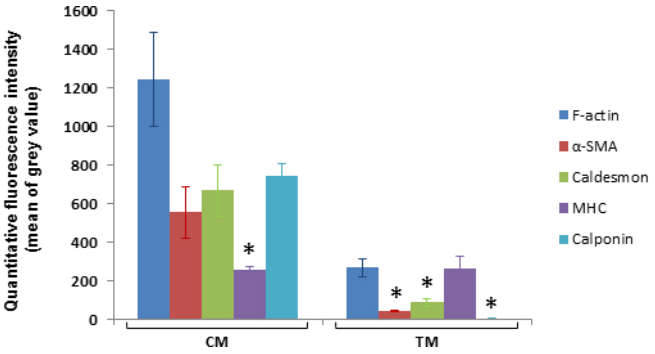

Figure 9. Fluorescence intensities of contractile markers in the trabecular meshwork (TM) and ciliary muscle (CM) based on quantitative analysis. Mean (±mean of standard error [SEM] error bars) fluorescence intensity (mean of grey pixel values in 8 region of interest (ROI) within TM or CM; n=3 mice per label) is represented by columns. In the CM, MHC mean fluorescence intensity was significantly less than that of F-actin ($p=0.02$). In the TM, mean fluorescence intensity was greatest for MHC and least for calponin. TM mean fluorescence intensities of α-SMA, caldesmon and calponin were less than that of F-actin and MHC ($p=0.0006$). Fluorescence intensities of F-actin and classic smooth muscle markers, caldesmon, α-SMA and calponin, were significantly higher in the CM compared with the TM ($p<0.0001$). MHC fluorescence intensity in the TM and CM was similar ($p>0.05$).

drainage system. The markers represented global contractility (F-actin), classic smooth muscle (α-SMA, caldesmon, and calponin), and nonmuscle contractile tissue epitopes (nonmuscle MHC).

Contractile epitopes were present throughout the anterior aqueous drainage tract in a profile and distribution that helped to distinguish the TM from the CM. F-actin labeling was seen in the TM and CM, with labeling intensity greater in the CM. Labeling of classic smooth muscle markers of α-SMA, caldesmon, and calponin was consistently strongly positive in the CM, and more intense compared with the TM. α-SMA, caldesmon, and calponin labeling was inconsistent and less intense in the TM. Nonmuscle MHC labeling was intense relative to other markers in the TM, but the converse was true for the CM. Our findings in BALB/c mice indicate that pigment, which was prominent in the CB of C57BL/6 mice, did not interfere with immunolocalization of smooth muscle markers in the adjacent CM in the mouse aqueous drainage tract.

Similar findings in primates have been reported. α-SMA is consistently present in the CM but inconsistently present in the TM, where it is inducible by transforming growth factor-beta [19-23]. Although cultured human TM cells are reported to express caldesmon [7,24], we are not aware of prior reports of caldesmon expression in the tissues of the CM or TM. Calponin expression has been reported in the CM [8,25], but to the best of our knowledge, the question of its presence in the TM has not been addressed. The presence of myosin in the aqueous drainage tract has been studied in human and porcine tissue [7,26], but its selectivity for TM is unreported. Overall, the observed profile of TM contractile epitopes supports the concept that the TM is a type of nonmuscle contractile tissue that also bears some features of smooth muscle.

The combined analysis of histology and differential labeling profiles of contractile markers provided insights into the organization of the mouse drainage tract, as depicted in Figure 10. The TM had anterior and posterior inner scleral regions. The anterior part of the TM was exposed to the anterior chamber. Here, the TM was a nonpigmented multilayered cellular structure bordering the corneal endothelial monolayer. Nearer the iris root, the anterior TM was pigmented. Both pigmented and nonpigmented regions of this anterior part of the TM were in contact with the anterior chamber.

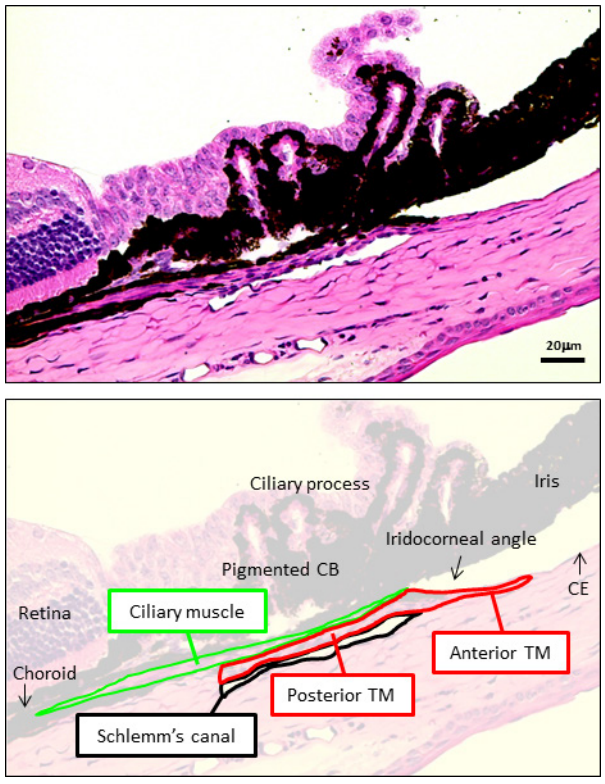

Figure 10. Organization of trabecular meshwork (TM) and cilliary muscle (CM) based on foregoing contractile marker localization studies of F-actin, MHC, α-SMA, caldesmon, and calponin in the mouse aqueous drainage tract. An anterior part of the TM faces the anterior chamber (anterior TM), while a more posterior part is sandwiched between CM and Schlemm's canal and does not face the anterior chamber (posterior TM). The CM extends from the iridocorneal angle of the anterior chamber to the anterior termination of retina posteriorly.

The pigmented TM lay anterior and immediately adjacent to SC in the inner sclera, analogous to the pigmented "filtering" TM of primates. The TM extended posteriorly from here as cellular layers alongside SC, sandwiched between SC and CM. This inner scleral TM was not directly in contact with the anterior chamber and could be considered analogous to the primate juxtacanalicular TM. SC virtually spanned the anterior-posterior length of the CB. We found that in postfixed specimens, SC is not always easily evident, as it may be closed or only partially open and slit-like. TM regions facing the anterior chamber (anterior) and inner scleral regions (posterior) adjacent to SC had identical contractile marker profiles.

The CM extended posteriorly from the iridocorneal angle as a fine tissue plane between TM cellular layers and the pigmented CB. The CM became more prominent posteriorly at the anterior termination of the retina and choroid. The mouse CM was longitudinally orientated and appeared smaller and simpler in three-dimensional configuration compared with that of primates. Equivalent versions of circular or radially orientated divisions of the primate CM were not immediately apparent in mice. The mouse CM has been described as lying posterior to the TM and SC [3,27], and our observations agree with this. We additionally observed, however, that the CM has an anterior extension from this posterior CM region, between tissue planes of the TM and pigmented CB, to the iridocorneal angle. This observation is important, as it is consistent with a continuous CM structure linking the anterior chamber anteriorly and a region of choroid and suprachoroidal space posteriorly. This organization provides a structural basis for uveoscleral outflow, and supports previous tracer studies hinting at this notion [12,28,29]. Functional studies to verify this postulation are beyond the scope of the present study but are planned for subsequent research.

Our approach of profiling contractile markers provided unique insights into the structural organization of the mouse aqueous drainage tract with respect to its contractile function. It allowed the apparently continuous structures of the TM and CM to be distinguished, revealing potential similarities and differences in the organization of the drainage tissues of primates and mice. That the contractile CM and TM are so intimately associated raises the possibility that their coordinated action helps to modulate aqueous outflow in mice, as likely also occurs in primates. Our findings provide important data for future studies seeking to understand and probe contractility in the aqueous drainage tract with reference to IOP and glaucoma.

ACKNOWLEDGMENTS

Special thanks to Murray Johnstone, MD for his expert comments on our manuscript. Grant support: National Institutes of Health, Bethesda, MD, Grants K08EY020863 (JCHT), P30EY03040 (Doheny Vision Research Institute Imaging Core), 1S10RR024754 (USC Multiphoton Core), and a Kirchgessner Foundation Research Grant (JCHT), American Glaucoma Society Mentoring for Physician Scientists Award and Young Clinician Scientist Award (JCHT), Career Development Award from Research to Prevent Blindness (JCHT), and an unrestricted grant from the Research to Prevent Blindness, Inc., New York, NY.

REFERENCES

1. Tian B, Gabelt BT, Geiger B, Kaufman PL. The role of the actomyosin system in regulating trabecular fluid outflow. Exp Eye Res 2009; 88:713-7. [PMID: 18793636].
2. Tian B, Geiger B, Epstein DL, Kaufman PL. Cytoskeletal involvement in the regulation of aqueous humor outflow. Invest Ophthalmol Vis Sci 2000; 41:619-23. [PMID: 10711672].
3. John SWM, Nishina PM, Sundberg JP. Systematic evaluation of the mouse eye, anatomy, pathology, and biomethods, CRC Press LLC;2002.
4. Tamm ER, Russell P, Piatigorsky J. Development of characterization of an immortal and differentiated murine trabecular meshwork cell line. Invest Ophthalmol Vis Sci 1999; 40:1392-403. [PMID: 10359321].
5. Wiederholt M, Thieme H, Stumpff F. The regulation of trabecular meshwork and ciliary muscle contractility. Prog Retin Eye Res 2000; 19:271-95. [PMID: 10749378].
6. Mao W, Liu Y, Wordinger RJ, Clark AF. A magnetic bead-based method for mouse trabecular meshwork cell isolation. Invest Ophthalmol Vis Sci 2013; 54:3600-6. [PMID: 23652493].
7. Inoue T, Pecen P, Maddala R, Skiba NP, Pattabiraman PP, Epstein DL, Rao PV. Characterization of cytoskeleton-enriched protein fraction of the trabecular meshwork and ciliary muscle cells. Invest Ophthalmol Vis Sci 2010; 51:6461-71. [PMID: 20631233].
8. de Kater AW, Shahsafaei A, Epstein DL. Localization of smooth muscle and nonmuscle actin isoforms in the human aqueous outflow pathway. Invest Ophthalmol Vis Sci 1992; 33:424-9. [PMID: 1740375].
9. Kashiwagi K, Lindsey JD, Kashiwagi F, Tsukahara S, Weinreb RN. Calponin distribution in human ciliary muscle and other anterior segment tissues. Invest Ophthalmol Vis Sci 1997; 38:349-56. [PMID: 9040467].
10. Gonzalez JM, Heur M, Tan JCH. Two-photon immunofluorescence characterization of the trabecular meshwork In Situ. Invest Ophthalmol Vis Sci 2012; 53:3395-404. [PMID: 22531697].

11. Aihara M, Lindsey JD, Weinreb RN. Aqueous humor dynamics in mice. Invest Ophthalmol Vis Sci 2003; 44:5168-73. [PMID: 14638713].

12. Lindsey JD, Weinreb RN. Identification of the mouse uveoscleral outflow pathway using fluorescent dextran. Invest Ophthalmol Vis Sci 2002; 43:2201-5. [PMID: 12091417].

13. Bárány EH. The immediate effect on outflow resistance of intravenous pilocarpine in the vervet monkey, Cercopithecus ethiops Invest Ophthalmol Vis Sci 1967; 6:373-80. .

14. Kaufman PL, Bárány EH. Loss of acute pilocarpine effect on outflow facility following surgical disinsertion and retrodisplacement of the ciliary muscle from the scleral spur in the cynomolgus monkey. Invest Ophthalmol Vis Sci 1976; 15:793-807. [PMID: 824222].

15. Bill A, Phillips CI. Uveoscleral drainage of aqueous humour in human eyes. Exp Eye Res 1971; 12:275-81. [PMID: 5130270].

16. Bill A. Effects of atropine and pilocarpine on aqueous humour dynamics in cynomolgus monkeys (Macaca irus). Exp Eye Res 1967; 6:120-5. [PMID: 4960736].

17. Gage PJ, Rhoades W, Prucka SK, Hjalt T. Fate maps of neural crest and mesoderm in the mammalian eye. Invest Ophthalmol Vis Sci 2005; 46:4200-8. [PMID: 16249499].

18. Tripathi BJ, Tripathi RC. Neural crest origin of human trabecular meshwork and its implications for the pathogenesis of glaucoma. Am J Ophthalmol 1989; 107:583-90. [PMID: 2729407].

19. Fuchshofer R, Tamm ER. The role of TGF-beta in the pathogenesis of primary open-angle glaucoma. Cell Tissue Res 2012; 347:279-90. [PMID: 22101332].

20. Han H, Wecker T, Grehn F, Schlunck G. Elasticity-dependent modulation of TGF-beta responses in human trabecular meshwork cells. Invest Ophthalmol Vis Sci 2011; 52:2889-96. [PMID: 21282571].

21. Nakamura Y, Hirano S, Suzuki K, Seki K, Sagara T, Nishida T. Signaling mechanism of TGF-beta1-induced collagen contraction mediated by bovine trabecular meshwork cells. Invest Ophthalmol Vis Sci 2002; 43:3465-72. [PMID: 12407157].

22. Pattabiraman PP, Rao PV. Mechanistic basis of Rho GTPase-induced extracellular matrix synthesis in trabecular meshwork cells. Am J Physiol Cell Physiol 2010; 298:C749-63. [PMID: 19940066].

23. Tamm ER, Siegner A, Baur A, Lutjen-Drecoll E. Transforming growth factor-beta 1 induces alpha-smooth muscle-actin expression in cultured human and monkey trabecular meshwork. Exp Eye Res 1996; 62:389-97. [PMID: 8795457].

24. Grosheva I, Vittitow JL, Goichberg P, Gabelt BT, Kaufman PL, Borras T, Geiger B, Bershadsky AD. Caldesmon effects on the actin cytoskeleton and cell adhesion in cultured HTM cells. Exp Eye Res 2006; 82:945-58. [PMID: 16679125].

25. Gaton DD, Sagara T, Lindsey JD, Weinreb RN. Matrix metalloproteinase-1 localization in the normal human uveoscleral outflow pathway. Invest Ophthalmol Vis Sci 1999; 40:363-9. [PMID: 9950594].

26. Zhang M, Rao PV. Blebbistatin, a novel inhibitor of myosin II ATPase activity, increases aqueous humor outflow facility in perfused enucleated porcine eyes. Invest Ophthalmol Vis Sci 2005; 46:4130-8. [PMID: 16249490].

27. Kogo H, Ito SY, Moritoki Y, Kurahashi H, Fujimoto T. Differential expression of caveolin-3 in mouse smooth muscle cells in vivo. Cell Tissue Res 2006; 324:291-300. [PMID: 16609918].

28. Kim TW, Lindsey JD, Aihara M, Anthony TL, Weinreb RN. Intraocular distribution of 70-kDa dextran after subconjunctival injection in mice. Invest Ophthalmol Vis Sci 2002; 43:1809-16. [PMID: 12036983].

29. Bernd AS, Aihara M, Lindsey JD, Weinreb RN. Influence of molecular weight on intracameral dextran movement to the posterior segment of the mouse eye. Invest Ophthalmol Vis Sci 2004; 45:480-4. [PMID: 14744888].

Articles are provided courtesy of Emory University and the Zhongshan Ophthalmic Center, Sun Yat-sen University, P.R. China. The print version of this article was created on 16 December 2013. This reflects all typographical corrections and errata to the article through that date. Details of any changes may be found in the online version of the article.